

# Electron and proton transfers modulate DNA binding by the transcription regulator RsrR.

Jason C. Crack,<sup>†,§</sup> Patricia Amara,<sup>‡,§</sup> Anne Volbeda,<sup>‡</sup> Jean-Marie Mouesca,<sup>§</sup> Roman Rohac,<sup>‡</sup> Ma Teresa Pellicer Martinez,<sup>†,§</sup> Chia-Ying Huang,<sup>§</sup> Océane Gigarel,<sup>‡</sup> Clara Rinaldi,<sup>‡</sup> Nick E. Le Brun<sup>†,\*</sup> and Juan C. Fontecilla-Camps<sup>‡,\*</sup>

<sup>†</sup>Centre for Molecular and Structural Biochemistry, School of Chemistry, University of East Anglia, Norwich Research Park, Norwich, NR4 7TJ, UK.

<sup>‡</sup>Univ. Grenoble Alpes, CEA, CNRS, IBS, Metalloproteins Unit, F-38044 Grenoble, France.

<sup>§</sup>Univ. Grenoble Alpes, CEA, CNRS, IRIG-DIESE-SyMMES-CAMPE, 38000 Grenoble, France.

<sup>§</sup>Macromolecular Crystallography, Swiss Light Source, Paul Scherrer Institute, 5232 Villigen PSI, Switzerland.

*Iron-sulfur cluster, proton-coupled electron transfer, transcription regulator, DNA regulation, redox sensor.*

---

**ABSTRACT:** The [Fe<sub>2</sub>S<sub>2</sub>]-RsrR gene transcription regulator senses the redox status in bacteria by modulating DNA binding while its cluster cycles between +1 and +2 states - only the latter binds DNA. We have previously shown that RsrR can undergo remarkable conformational changes involving a 100° rotation of tryptophan 9 between exposed (**Out**) and buried (**In**) states. Here, we have used the chemical modification of Trp9, site-directed mutagenesis and crystallographic and computational chemical studies to show that (i) the **Out** and **In** states correspond to oxidized and reduced RsrR, respectively, (ii) His33 is protonated in the **In** state due to a change in its pK<sub>a</sub> caused by cluster reduction and (iii) Trp9 rotation is conditioned by the response of its dipole moment to environmental electrostatic changes. Our findings illustrate a novel function of protonation resulting from electron transfer.

---

## INTRODUCTION

Every living organism is subjected to environmental stresses, such as UV light, drought or nutrient scarcity and these are especially severe in the case of unicellular microbes. This barrage of stresses has resulted in the evolution of a myriad of gene products that function to minimize the effects of these hostilities. It is, however, economically essential to restrict their production to when they are needed. In bacteria, this gene regulation typically depends on a diverse array of proteins, some of which belong to the Rrf2 superfamily of dimeric bacterial transcription regulators.<sup>1</sup> Many, but not all, members of this superfamily use [Fe-S] clusters as sensors: [Fe<sub>2</sub>S<sub>2</sub>]-IscR senses the [Fe-S] cluster status of the cell,<sup>2</sup> [Fe<sub>4</sub>S<sub>4</sub>]-RirA detects iron limitation,<sup>3</sup> [Fe<sub>4</sub>S<sub>4</sub>]-NsrR detects the presence of nitric oxide (NO)<sup>4</sup> and [Fe<sub>2</sub>S<sub>2</sub>]-RsrR appears to sense the redox status of the cell.<sup>5</sup> The cluster coordination is remarkably variable: IscR is thought to have three Cys and one His cluster ligand,<sup>6</sup> RirA may have only three Cys cluster ligands,<sup>7</sup> NsrR has three Cys and one Asp cluster ligands<sup>8</sup> and RsrR is the most unusual one with one His, one Glu and two Cys cluster ligands.<sup>9</sup> High resolution crystal structures are available for apo-IscR, both alone and in complex with DNA,<sup>10,11</sup> and for the holo forms of NsrR and RsrR; the latter two solved by us.<sup>8,9</sup> They all form elongated dimers with the [Fe-S] clusters positioned close to either end. In the case of NsrR and RsrR the clusters are coordinated by ligands from both monomers.

Previous work by some of us has determined that RsrR from *Streptomyces venezuelae* (*Sv*) binds with high affinity to its two classes of DNA sites only when its [Fe<sub>2</sub>S<sub>2</sub>] cluster is oxidized.<sup>5</sup>

Consistent with this observation, the protein readily cycles between 1+ and 2+ redox states. These characteristics underpin the central role the cluster plays and raises the question of how a one electron redox process can generate the conformational changes necessary to elicit or prevent DNA binding. As far as we are aware, this is a unique process in biology: in all other cases of transcriptional regulation in which an [Fe-S] cluster acts as the sensory unit, and which involves the loss or gain of regulator protein DNA binding, the sensing reaction involves significant changes at, or loss of, the cluster. Examination of the *Sv*RsrR cognate DNA sites suggests that this protein is involved in both the regulation of the relative cell concentrations of NADH and NAD(P)H and the synthesis of mycothiol (1D-myoinositol 2-(N-acetyl-L-cysteinyl)amido-2-deoxy- $\alpha$ -D glucopyranoside) precursors. Mycothiol is the Actinobacterial equivalent of the ubiquitous antioxidant glutathione.<sup>12</sup>

We have recently reported the crystal structures of *Sv*RsrR in the oxidized (Figure 1a), partially reduced and fully reduced states.<sup>9</sup> We found that in the partially reduced state the protein crystallizes as dimers containing monomers with different conformations in the vicinity of the [Fe<sub>2</sub>S<sub>2</sub>] cluster, which is bound at the dimer interface. In one of these monomers, Trp9 displays a solvent-exposed position we called **Wo**, and in the other one this residue is buried in a protein cavity adopting a conformation we called **Wi** (Figure 1b). Here, we have extended our definition of the two forms to “**Out**” and “**In**”, respectively, to encompass the correlated changes of the “half-dimer” structure (Figure 1). The most evident difference between these two conformations can be modeled as an approximate 100° rotation

about the Trp9  $\alpha$ -C $\beta$  bond. As a consequence, the DNA-binding helix-turn-helix motif of SvrSsrR also adopts different orientations in the two monomers. Another significant change is a shift of about 1.5 Å of the His33 imidazole ring (Figure 1b).

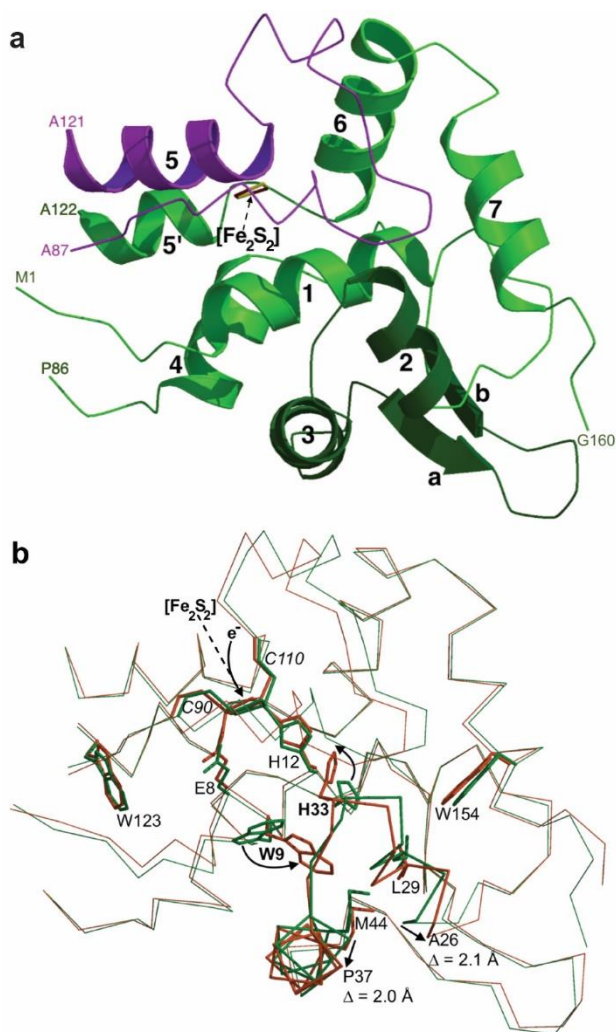


**Figure 1.** A SvrSsrR half-dimer with the  $[\text{Fe}_2\text{S}_2]$  cluster at the interface of the two monomers. The half-dimer for which structure superpositions provide a better fit is defined by residues 1 to 86 and 122 to 160 from one monomer and by residues 87 to 121 from the other. **a** Secondary structure elements of the monomer in the **Out** form (green; the segment of the other monomer is shown in purple). Ribbons depict  $\alpha$ -helices and arrows indicate  $\beta$ -strands. **b**  $\text{C}\alpha$  superposition of the **Out** and **In** forms. Black arrows indicate major movements. Selected residues are shown as sticks.  $\text{C}\alpha$ -traces and corresponding labeled residues are uniformly colored green for the **Out** form and orange for the **In** form. The DNA binding helix-turn-helix motif is highlighted with thicker lines.

Because the indole ring of tryptophan possesses a dipole moment, we next speculated that the two observed Trp9 conformations could result from the two redox states of the  $[\text{Fe}_2\text{S}_2]$  cluster. Fully oxidized and fully reduced SvrSsrR crystallize in the same  $\text{P}2_1$  space group with very similar cell parameters and both have their monomers in the **Out** conformation.<sup>9</sup> This situation, which we showed is most likely caused by crystal pack-

ing forces, excluded the possibility of using X-ray crystallography to characterize the possible relation between Trp9 conformation and redox state. Here, we provide evidence from both chemical modification experiments and the medium-resolution crystal structure of a SvrSsrR-DNA complex that supports the assignment of **Out** and **In** to the oxidized and reduced states, respectively. In order to investigate the cause of His33 conformational changes between the **In** and **Out** forms and their possible functional role (Figure 1b), we have (i) performed a series of molecular dynamics and metadynamics simulations in order to explore its possible (double) protonation upon cluster reduction, (ii) substituted His33 with Ala, characterized this variant's phenotype and solved its high-resolution crystal structure and (iii) run pH-dependent EMSAs of both wild type SvrSsrR and its H33A variant. Furthermore, we have calculated the response of Trp9's dipole to electrostatic changes during the **Out** to **In** transition. Taken together, our results provide strong support for a remarkable mechanism, in which either sequential or correlated electron and proton transfers drive redox-dependent conformational changes that modulate DNA binding by SvrSsrR.

## RESULTS.

**Chemical modification of Trp9 in the W123F/W154F-SvrSsrR double variant.** In order to try to correlate redox state and Trp9 conformation we decided to carry out the chemical modification of this residue in both oxidized and reduced SvrSsrR. To minimize potential for ambiguity, the two additional Trp residues of SvrSsrR (Trp123 and Trp154 (Figure 1b)) were replaced by Phe (W123F/W154F-SvrSsrR). The UV-visible absorbance and CD spectra of the reduced and oxidized variant were very similar to those of the wild type protein (Figures S1a and S2a) and air oxidation and dithionite reduction showed that its cluster also can undergo redox cycling. Like the wild type protein, only the oxidized form of W123F/W154F-SvrSsrR variant binds DNA (Figures S1b and S2b).

Trp can be formylated by chloroform upon exposure to UV light in a photochemical reaction that does not depend on the presence of  $\text{O}_2$ <sup>13,14</sup> (Figure 2a). Irradiation at 280 nm for 60 min of a solution containing chloroform and reduced W123F/W154F-SvrSsrR resulted in changes in the CD spectrum, reflecting limited (~15%) cluster oxidation (Figure 2b). In contrast, no significant change was observed in the CD spectrum of oxidized W123F/W154F-SvrSsrR post irradiation (Figure 2c). In order to determine the extent of formylation in oxidized and reduced SvrSsrR variants, samples were analyzed by liquid chromatography electrospray ionization mass spectrometry (LC-ESI-MS). As expected, the deconvoluted spectra of all samples were dominated by the apo-SvrSsrR peak at 17285.1 Da (theoretical mass of 17285.9 Da) because the  $[\text{Fe}_2\text{S}_2]$  cluster is lost under the acidic conditions of LC-ESI-MS sample preparation (Figure 2d). The mass spectrum of non-treated, as-isolated SvrSsrR contains a series of broad, but poorly resolved adduct peaks on the high mass side. Following chloroform/irradiation, a prominent peak at +28 Da, as expected from the addition of a -CHO group to the indole ring,<sup>13,15</sup> was observed in the spectrum of oxidized SvrSsrR. The same adduct peak was found in the spectrum of the reduced sample, but at a much lower relative abundance (Figure 2d).

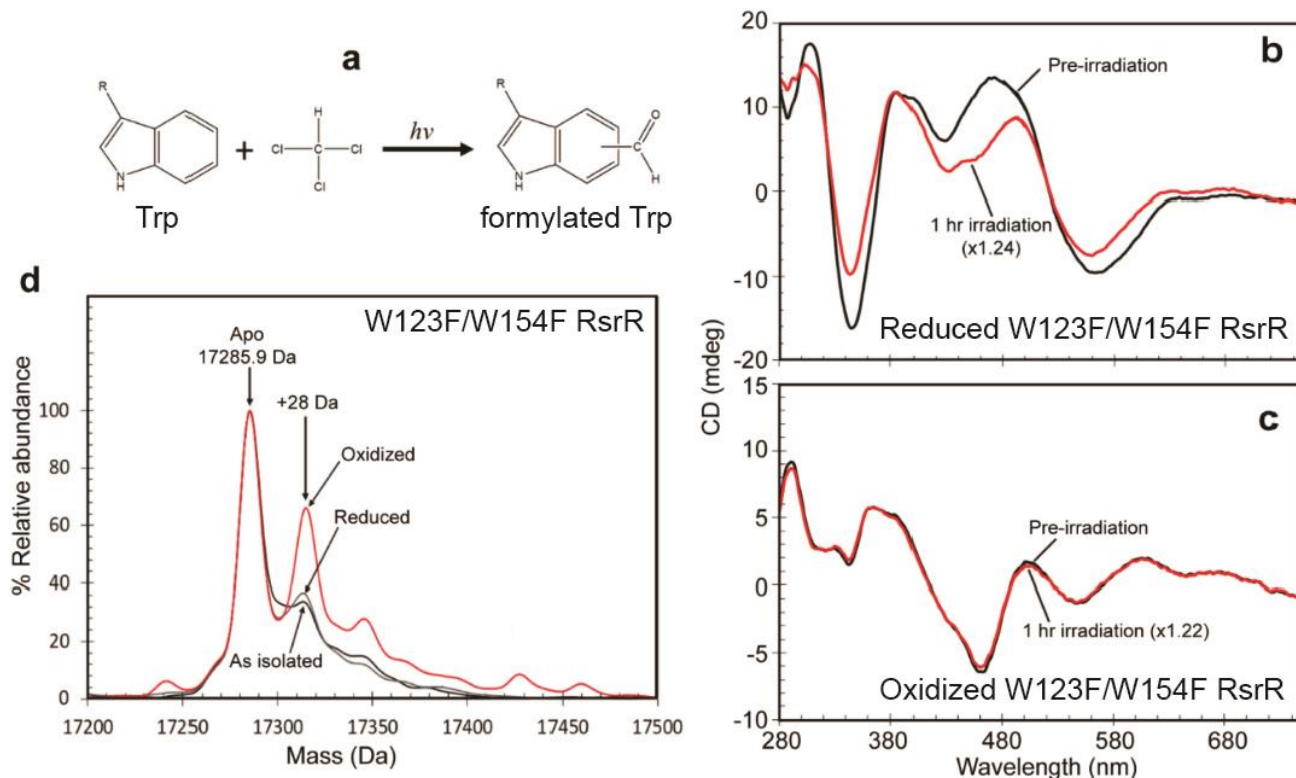


**Figure 2.** Redox-dependent modification of Trp9 by chloroform/irradiation. **a** The modification reaction which results in formylation of the Trp side chain. **b** CD spectra of as isolated (reduced) W123F/W154F SvRsrR (~100  $\mu$ M cluster) in chloroform-saturated 250 mM ammonium acetate, pH 7.5, prior to (black) and following a 1 hr irradiation at 280 nm (red). The post irradiation spectrum was multiplied as indicated to account for loss of protein due to some precipitation during exposure to UV-light. **c** As in **b** except that the  $[\text{Fe}_2\text{S}_2]$  cluster was in the oxidized state. **d** Deconvoluted LC-ESI-MS of the as isolated (reduced) untreated sample and of the reduced and oxidized chloroform-treated samples following 1 hr irradiation.

To confirm the origin of the +28 Da peak, trypsin digested samples were analyzed by LC-MS and MS/MS. This procedure revealed the presence of a large, multiply charged, but unmodified tryptophan-containing peptide that was common to all samples (Figure S3). Conversely, the oxidized sample also contained an equivalent peptide but with a gain of 28.24 Da, consistent with the formylation of Trp9. The same formylated peptide was observed in the reduced sample but at a significantly lower (~7-fold less) abundance (consistent with the differences observed in Figures 2b and 2d for the whole protein). Importantly, the modified peptide was absent from untreated/non-irradiated samples. The observed difference in the accessibility of Trp9 to formylation between oxidized and reduced  $[\text{Fe}_2\text{S}_2]$ -SvRsrR samples is entirely consistent with a redox-linked conformational change, in which its side chain becomes more accessible (i.e. **Wo**) when the cluster is in the oxidized state.

#### Medium resolution structure of a SvRsrR-DNA complex.

In order to obtain structural information on SvRsrR DNA binding, a complex between air-oxidized SvRsrR and a 39 DNA base-pair fragment was crystallized in two different space groups (called complex 1 and 2 in Table S1). The sequence of the two complementary strands, which corresponds to one previously used in EMSA experiments,<sup>5</sup> is shown in Figure 3a.

In agreement with the chemical modification studies (Figure 2), no molecular replacement (MR) solution was obtained with X-ray data from complex 1 when starting from two half-dimers in the **In** conformation (Table S2). Conversely, when half-dimers in the **Out** conformation were used (with the  $[\text{Fe}_2\text{S}_2]$  cluster omitted), a normal dimer was recovered with significant

$F_o - F_c$  omit map electron density for the cluster (Table S2). After adding two manually-built 15 base pair-long ideal B-DNA search models, an improved MR solution was obtained in which the two DNA fragments form a continuous 30 base-pair double helix. This structure was next used as a starting model to carry out a new MR search for complex 2 (Table S2), which showed the presence of four copies of the SvRsrR-DNA complex in its asymmetric unit and about 50% twinning. Subsequently, a combination of cross-crystal electron density averaging, real space refinement against the resulting averaged map, several manual model corrections and reciprocal space refinement using X-ray data from complex 1 produced a 4.3 Å resolution model (Figure 3a) with an  $R_{\text{free}}$  of 30.0% and correct geometry. Starting from this model similar refinement statistics were obtained for complex 2 using data to 4.1 Å resolution (Table S3).

The cross-crystal averaged electron density map shows that much of the DNA and RsrR structure is reasonably well resolved (Figure S4). In the refined model the large and small groove of the DNA double helix are occupied by  $\alpha$ -helix 3 (residues 36-48) and part of the downstream  $\beta$ -hairpin of SvRsrR, respectively (Figure 3a). Additional interaction points involve residues around the N-termini of  $\alpha$ -helices 1 and 2. There is just a small rearrangement of **Out** half-dimers in the complex compared to the structure of the non-complexed **Out** dimer. Conversely, a contact analysis of the superimposed **In** dimer shows many collisions (Table S4).

A concerted movement of His33, Trp9 and Tyr39, which sit in well-defined electron density (Figure 3b), represents one of

the more significant differences between uncomplexed and complexed **Out** forms (Figure 3a). This change is explained by (i) the shift of Tyr39 towards the DNA backbone where it establishes an H-bond with a phosphate group, (2) a rotation of Trp9 into the space liberated by Tyr39 and (3) a shift of His33 within the protein cavity. As a result, Tyr39 is the residue that makes the most contacts with the DNA fragment and Trp9 is also in Van der Waals contact with it (Table S4).

**His33 of *SvRsrR* plays an important role in the Out-to-In transition.** Because the orientation of His33 changes significantly in going from the **Out** to the **In** conformation (Figure 1b), we investigated its protonation state in the two forms using molecular dynamics (MD). We constructed the two models observed in the crystal structures: an **Out/Out** dimer and a mixed **In/Out** dimer.<sup>9</sup> In each model, we focused our analysis on one **Out** monomer from the former and the **In** monomer from the latter (see Methods and Supporting Information for details). Accordingly, the names of our models will only refer to the monomer we will be discussing.

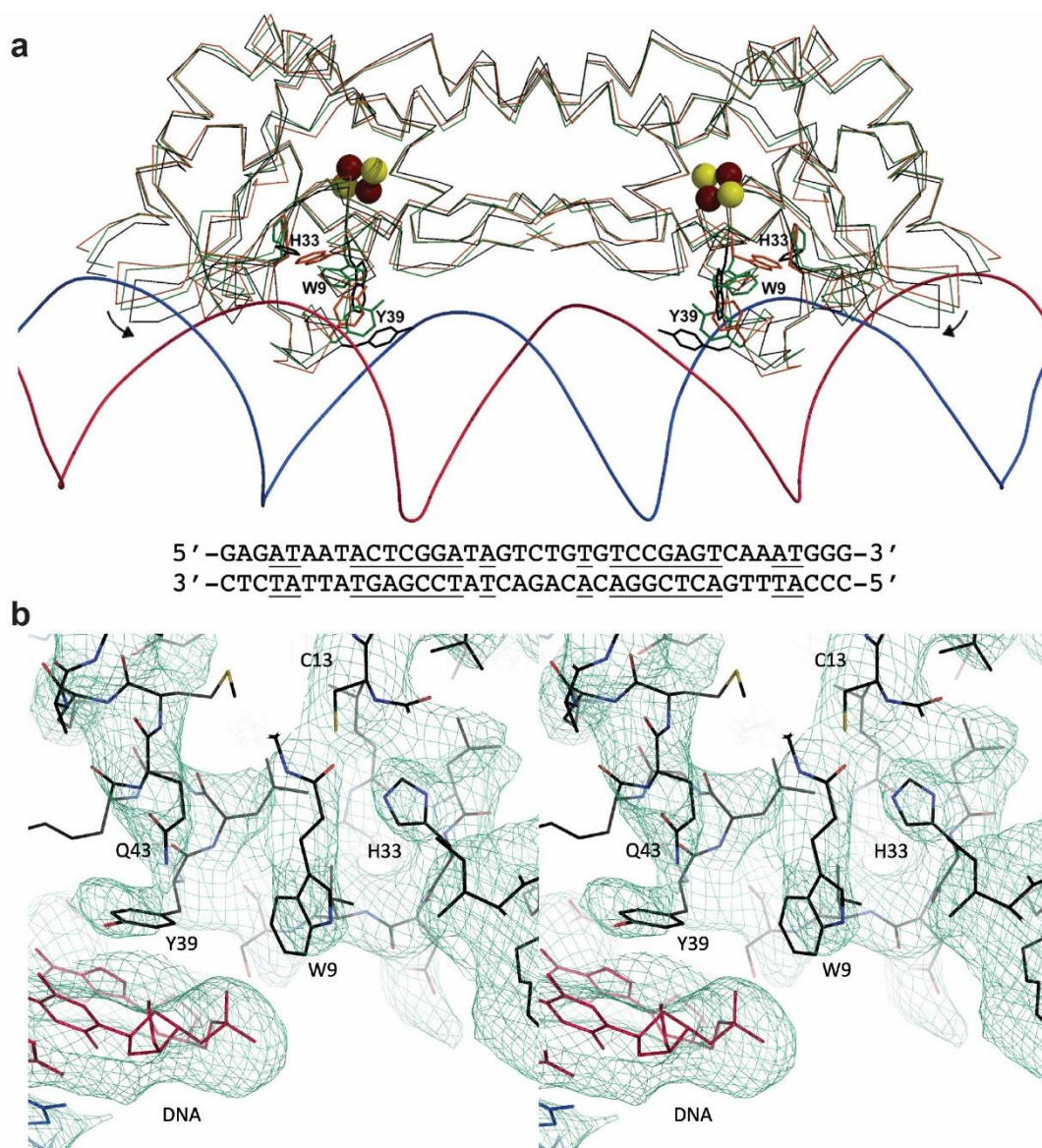


**Figure 3.** Structure of a complex of *SvRsrR* with a 39 base pair cognate DNA fragment. **a** Overall view of the structure with the sequence of the complementary DNA strands used for crystallography given below it (bases with palindromic symmetry are underlined). The  $C\alpha$ -traces of the two *SvRsrR* subunits are shown in black and the phosphate backbones of the bound DNA strands are depicted in blue and crimson. The superimposed  $C\alpha$ -traces of the uncomplexed oxidized **Out** and reduced **In** forms are depicted in green and orange, respectively; the arrows indicate a small rotation of the corresponding half-dimers from the uncomplexed **Out** to the complexed *SvRsrR* form. **b** Cross-eyed stereo image of the protein region around Trp9, His33 and Tyr39 and a small fraction of DNA (the cross-crystal averaged electron density is shown as a light-blue mesh contoured at 0.8 r.m.s. value of the map). For *SvRsrR* the following atom colors are used: C black, N blue, O red and S yellow. The two DNA strands are uniformly colored in crimson and blue.

As shown by the Trp9 chemical modification studies reported above, it is clear that the  $[\text{Fe}_2\text{S}_2]$  cluster is oxidized in the **Out** conformation (**Out/Ox**) and reduced in the **In** conformation (**In/Red**). In the **Out/Ox** state, the experimentally observed hydrogen bond between the N $\delta$ 1 of His33 and the carbonyl oxygen of Leu29, as well as the local conformation, are mostly maintained during the MD simulation when His33 is neutral (**H33<sup>0</sup>**, Figures 4a and 4c). Only in a few frames does the His33 side chain rotate and make a hydrogen bond with a water molecule (Figure S5). In contrast, the His33-Leu29 hydrogen

bond is immediately lost when His33 is protonated in our starting model (**H33<sup>+</sup>**, Figure 4b). Interestingly, in the MD simulations the positively charged His33 side chain approaches the cluster, adopting a position close to the one it occupies in the crystallographic **In** form (Figure 1b). This movement creates a cavity that becomes filled with water from the solvent medium (Figure S6). We therefore conclude that the **Out** conformation of SvRsrR very likely corresponds to the **Out/Ox/H33<sup>0</sup>** state.

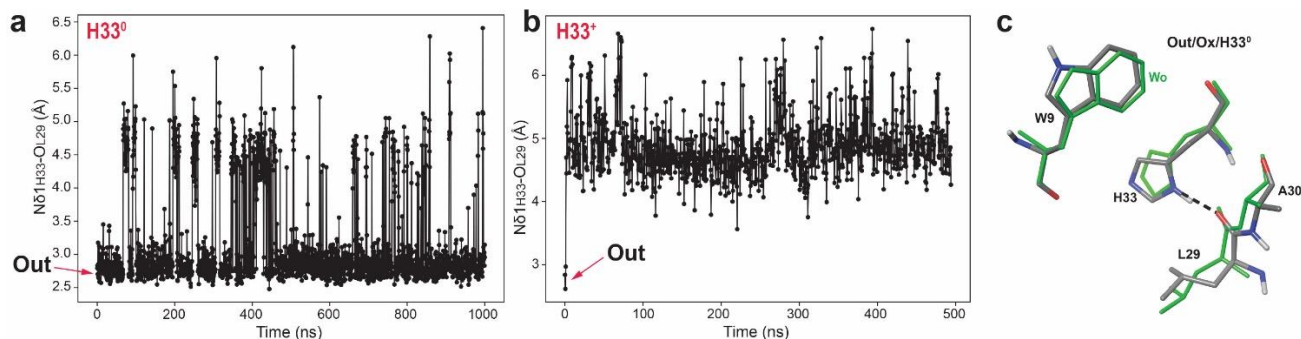


**Figure 4.** Molecular dynamics simulations of the **Out/Ox** model. Variations of the distance between the N $\delta$ 1 atom of His33 and the O atom of Leu 29 during the MD simulation of the **Out/Ox** form with **a**, neutral His33 with a proton on N $\delta$ 1 (**H33<sup>0</sup>**) and **b**, positively charged His33 with protons on N $\delta$ 1 and N $\epsilon$ 2 (**H33<sup>+</sup>**). **c** Typical frame extracted from the trajectory of the **Out/Ox/H33<sup>0</sup>** state superimposed on the **Out** crystal structure (green atoms); for the calculated model C, N, O and H atoms are colored gray, blue, red and white, respectively. Only polar hydrogens are represented for clarity. Moreover, only residues around His33 are depicted because in both cases the rest of the protein is very similar to that of the **Out** crystal structure.

When the **In/Red** conformation is modeled with a neutral His33, the local conformation around Trp9, Leu29 and His33 is disrupted after 100 ns (Figure 5a); the structural water molecule that binds to these three residues is definitely lost and His33 adopts three conformations which are not observed in the corresponding crystal structure (Figure S7). Conversely, the crystallographically-observed **In/Red** conformation is best reproduced with a protonated His33. Indeed, the hydrogen

bonds that a single water molecule establishes with the above three residues are maintained for most of the dynamics (Figure 5b). Remarkably, although this water molecule is constantly exchanged during the first 600 ns, in the last 400 ns of the simulation the same water remains fixed in the conformation observed in the **In/Red** X-ray model (Figure 5c). We conclude that the **In** conformation very likely corresponds to the **In/Red/H33<sup>+</sup>** state.

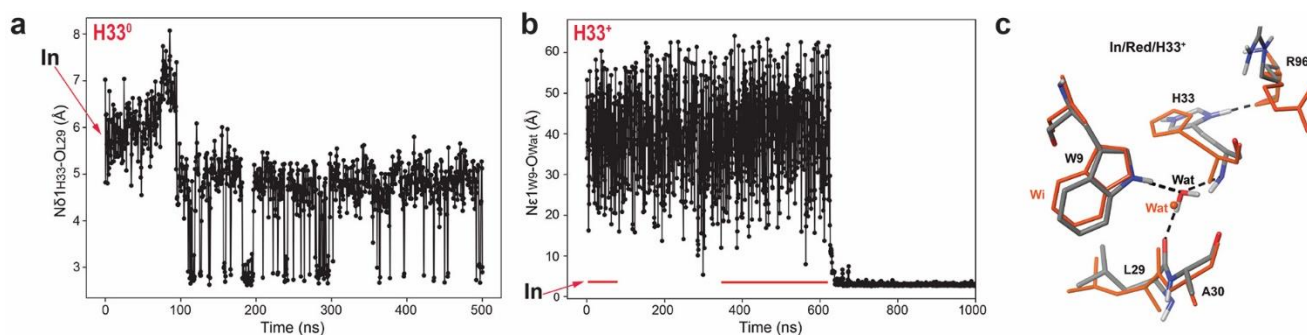


**Figure 5.** Molecular dynamics simulations of the **In/Red** models. **a** Variation of the distance between the N $\delta$ 1 atom of His33 and the O atom of Leu 29 during the MD simulation of the **In/Red** form with a neutral His33 with a proton on N $\delta$ 1 (**H33<sup>0</sup>**). **b** Monitoring of the presence of the water molecule H-bonded to Trp9, Leu29 and His33 in the **In/Red/H33<sup>+</sup>** model. The two red lines highlight the frames where a water molecule is present, exchangeable with the solvent; for the last 400 ns the same water molecule is bound at that site. **c** Typical frame extracted from the last 400 ns (see **b**) of the MD trajectory of the **In/Red/H33<sup>+</sup>** state superimposed on the SvRsrR **In** crystal structure (orange atoms). In **c**, for the calculated model C, N, O and H atoms are colored gray, blue, red and white, respectively. Only polar hydrogens are represented for clarity. Moreover, only residues around His33 are depicted because in both cases the rest of the protein is very similar to that of the **In** crystal structure.

Molecular dynamics cannot be used to monitor the transition between the **Out/Ox** and **In/Red** conformations because it would require inaccessible computational times. We therefore

employed instead the metadynamics method that allows an enhanced sampling of the so-called collective variables that best describe the conformational change of interest.<sup>16,17</sup> We chose to use two collective variables: the dihedral angle  $\varphi$  ( $\text{C}\gamma\text{-C}\beta\text{-C}\alpha$ -

C) to sample the rotation of the Trp9 side chain upon going from **Wo** to **Wi** (X-ray values:  $\varphi_{\text{out}} = 165^\circ$  and  $\varphi_{\text{in}} = 65^\circ$  (Table S5) and the distance **d** between the C $\eta$ 2 atom of the Trp9 benzene ring and the C $\beta$  of Met44 (X-ray values:  $\mathbf{d}_{\text{out}} = 13 \text{ \AA}$  and  $\mathbf{d}_{\text{in}} = 6 \text{ \AA}$ ) (See Figure 1b and Methods for details). In agreement with experiment, a 250 ns simulation starting with the **Out/Ox/H33<sup>0</sup>** state indicates that the region characterized by  $\varphi_{\text{out}} = 165^\circ$  and  $\mathbf{d}_{\text{out}} = 13 \text{ \AA}$  (the **Out** form) corresponds to a minimum. In contrast, the region corresponding to the **In** form, with collective variables  $\varphi_{\text{in}} = 65^\circ$  and  $\mathbf{d}_{\text{in}} = 6 \text{ \AA}$ , is not a minimum in this case (Figure S8). Adding one electron to the [Fe<sub>2</sub>S<sub>2</sub>] cluster of **Out/Ox/H33<sup>0</sup>** to get **Out/Red/H33<sup>0</sup>** changes the energy profile and the **In** region becomes slightly lower in energy (Figure 6a). Conversely, when in the starting model His33 is protonated (**Out/Red/H33<sup>+</sup>**) the zone defined by the collective variables corresponding to the **In** form is found now at an energy minimum (Figure 6b). Remarkably, when a frame extracted from this region is superimposed on the crystal **In** form, it becomes clear that the crucial changes observed between the **Out** and **In** conformations have been closely reproduced with the metadynamics procedure (Figure S9 and Figure 1b). In addition, a molecular orbital analysis of the effect of [Fe<sub>2</sub>S<sub>2</sub>] cluster reduction on His33 further indicates that, as expected, the pK<sub>a</sub> of this residue should become more basic, facilitating its subsequent protonation (Figure S10).

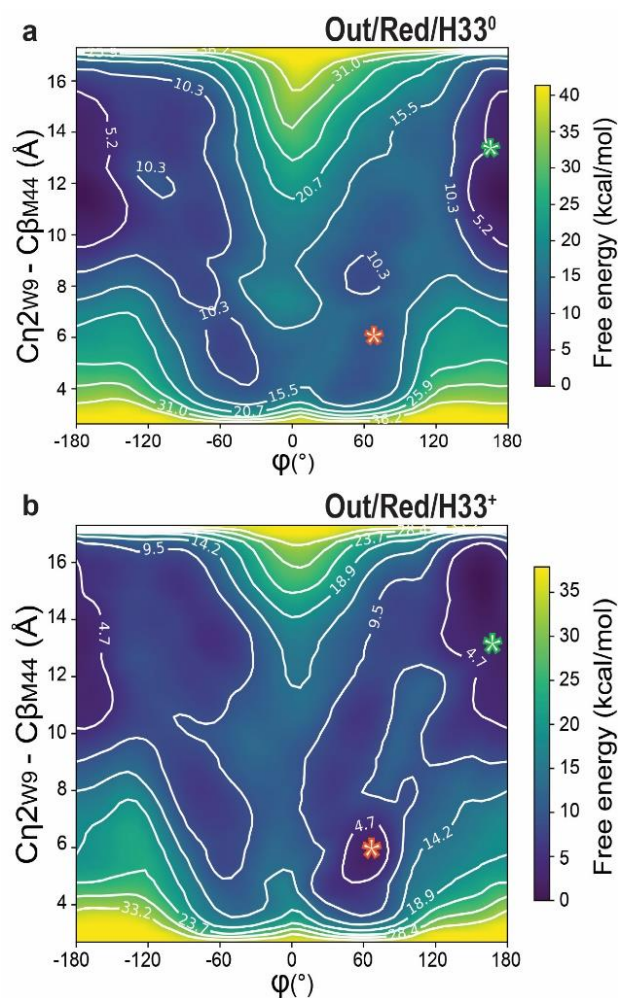


**Figure 6.** Free energy surface resulting from a 250 ns metadynamics simulation run starting from **a**, the **Out/Red/H33<sup>0</sup>** and **b**, the

**Out/Red/H33<sup>+</sup>** state. The green and orange stars on the plots indicate the values of collective variables  $\varphi$  and **d** for **Wo** and **Wi**, respectively (see text). A minimum is observed in the orange starred (**Wi**) region only when His33 is protonated.

**Response of the Trp9 side chain dipole to electrostatic changes.** To investigate whether the protonation of His33 could also have a direct effect on the Trp9 dipole response and the **Wo/Wi** transition (Figure 1b), we computed the electrostatic energy profile by rotating the Trp9 side chain about the C $\alpha$ -C $\beta$  bond, corresponding to  $\varphi$  (Figure 7a). The electrostatic contribution to the **Wo/Wi** transition of (i) the atomic charges of the cluster, (ii) the positive charge of protonated His33 and (iii) the net charges of surrounding residues modeled as point charges were considered in the calculation (see Figure 7a and Supporting Information). Although we have explored the whole  $\varphi$  range, we will focus our attention on the  $[\varphi_{\text{in}} - \varphi_{\text{out}}]$  angular range.

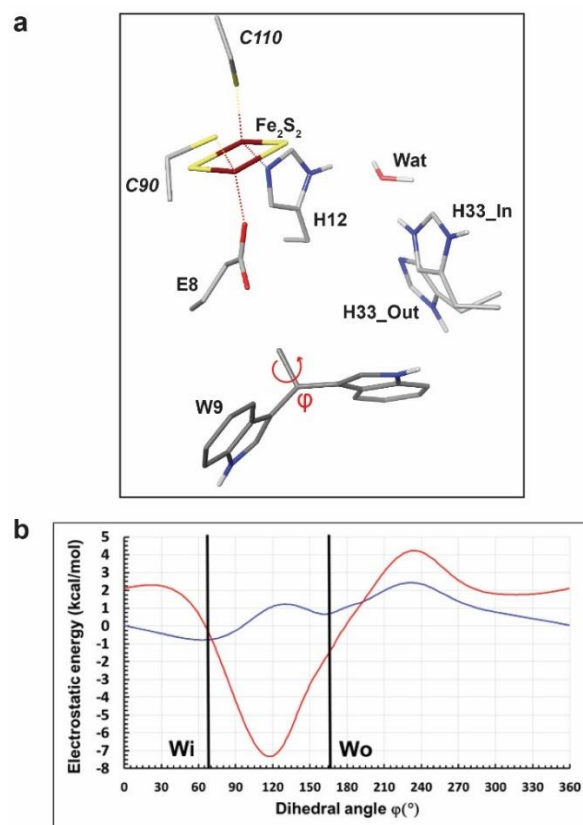


**Figure 7.** **a** Minimal atomic model used for electrostatic calculations showing both neutral (**Out/Ox/H33<sup>0</sup>**) and protonated (**In/Red/H33<sup>+</sup>**) His33 positions. Trp9 is rotated about its C $\alpha$ -C $\beta$  bond (red arrow) in order to explore its electrostatic interaction with the surrounding charges (see Supporting Information for details). **b** electrostatic energy profiles for both **Out/Ox/H33<sup>0</sup>** (blue line) and **Out/Red/H33<sup>+</sup>** (red line) obtained by rotating Trp9. Vertical lines highlight the  $\varphi$  values that match **Wo** and **Wi**.

First, for the **Out/Ox/H33<sup>0</sup>** state, the interaction of the charge distribution with the Trp9 dipole shows two minima that correspond to **Wo** and **Wi** (Figures 7b and S11). This indicates that the electrostatic energy contributes to the local stabilization of the two Trp9 rotamers that are the most frequently found for this residue in proteins (Table S5). The reduction to **Out/Red/H33<sup>0</sup>** significantly deepens the two minima due to the

addition of a negative charge to the cluster (Figure S12). In addition, the protonation of His33 that leads to the **Out/Red/H33<sup>+</sup>** state creates a well between **Wo** and **Wi** (Figures 7b, S13 and S15), indicating that the overall barrier between these conformations is lowered.

**Dependence of the His33-[Fe<sub>2</sub>S<sub>2</sub>] interaction on the redox state of SvRsrR.** The electrostatic energy of the His33–cluster interaction that we used as a reference in the **Out/Ox/H33<sup>0</sup>** form was set to 0 kcal/mol. The following relative energies are given with a dielectric constant of 1 since its actual value is unknown (see Supporting Information). Here, we are only interested in the trends they provide. Thus, reducing the cluster by one electron and protonating His33, without shifting its position to the **In** conformation, yields an attractive interaction with an electrostatic energy of -48 kcal/mol (comment in Figure S13). The calculated value for the His33–cluster interaction in the **In/Red/H33<sup>+</sup>** state is -69 kcal/mol (comment in Figure S14), giving a driving force for the observed shift of His33 towards the cluster of -21 kcal/mol (Figure 1b). This shift creates a cavity into which Trp9 can now rotate while going from **Wo** to **Wi**. The Trp9 side chain in the **In** form is further stabilized by its interaction with a water molecule that, as mentioned above, also forms H-bonds with Leu29 and His33 (Figure 5c).

**Trp9 chemical modification in the H33A variant.** To further study the role of His33 in the **Out** to **In** conformational change we prepared and characterized a SvRsrR H33A variant. Both UV-visible absorbance and CD spectra of as isolated (reduced) H33A-SvRsrR were indistinguishable from those of the wild type protein (Figure S16a), and exposure to O<sub>2</sub> resulted in cluster oxidation that could be readily reversed upon addition of reductant, i.e. the H33A variant can redox cycle as the wild type protein. The CD spectrum of oxidized H33A-SvRsrR is distinct from that of the wild type protein suggesting, as expected from examination of the wild type SvRsrR crystal structure, that this residue is sensed by the [Fe<sub>2</sub>S<sub>2</sub>] cluster environment. EMSA studies of H33A-SvRsrR revealed that in its oxidized form the variant binds DNA like the wild type protein does (Figure S16b). Importantly, the reduced form of H33A-SvRsrR retained significant capacity to bind DNA (Figure S16b), demonstrating that the connection between cluster redox state and its influence on the DNA-binding conformation is severely affected in this variant.

Like in the native protein, chloroform had no effect on the CD spectra of either the oxidized or reduced H33A variant and irradiation at 280 nm for 60 min caused some cluster oxidation in the reduced sample (Figure S17). However, LC-ESI-MS analysis before and after chloroform/UV treatment revealed a significant formylation adduct at +28 Da in *both* redox states (Figure S16c) indicating that reduction does not lead to a major loss of the solvent exposure of Trp9 in the H33A variant. Consequently, the conformational change to the **In** state, which results from reduction of the wild type protein, does not seem to occur in this variant (see also next section). This is consistent with the fact that, as indicated above, its ability to bind DNA in its cluster-reduced form is preserved to a significant degree (Figure S16b).

**H33A variant 1.68 Å resolution crystal structure.** Monoclinic crystals of the dithionite-reduced H33A-SvRsrR variant were obtained anaerobically with conditions very similar to those used for the orthorhombic P2<sub>1</sub>2<sub>1</sub>2<sub>1</sub> form of the wild type protein<sup>9</sup> (third crystal in Table S1). There are two H33A-SvRsrR dimers in the crystal asymmetric unit. One of the mon-

omers of each dimer is in a conformation practically indistinguishable from the **Out** form of the wild type protein, here called **Out-like** (Figure S18). In each dimer the other monomer has Trp9 in a buried conformation, with the occupancy set to 1.0 in one case and 0.7 in the other. However, this conformation, that we will call **In-diff** and which may be favored by the absence of the His33 side chain, differs significantly from the wild type **In** form (Figure S19). Notably, it lacks the structural water molecule that interacts with Trp9 in the latter (Figure 5c). This may explain why, according to both the chemical modification and EMSA studies reported in the previous sections, the **In-diff** conformation appears to be less stable in solution. Examination of the crystal contacts in the vicinity of the helix-turn-helix DNA-binding motif of H33A-SvRsrR shows that both **Out-like** monomers have the same interactions between the loop containing residues 34–39 and the residues from a symmetry-related counterpart. The same is true for the two **In-diff** monomers. However, the interactions for **Out-like** monomers differ strongly from those for **In-diff** monomers. Thus, crystal contacts play a determinant role in positioning helix 3 (Figure 1a). In the **In-diff** monomers, helix 3 is displaced relative to Trp9 in the **In** form by 3.1 Å at the Tyr39 position (Figure S19) creating a large cavity. Analysis of the structure suggests that in the **In-diff** monomers a rotation of the Trp9 side chain towards the solvent should be possible, since this motion would not be hindered. Conversely, the opposite rotation of this residue in the **Out-like** monomers towards the protein cavity would result in clashes with the side chains of residues Cys13, Ala33, Leu40 and Gln43. This might explain why in one of the **In-diff** monomers Trp9 adopts a solvent-exposed conformation with 0.3 occupancy. In summary, our H33A-SvRsrR crystal structure shows that the His-to-Ala substitution has a major impact in the organization of the protein cavity that lodges Trp9. In addition, the average temperature factors (B) of the Trp9 side chain in the variant are significantly higher in the **In-diff** form than in the **Out-like** form (43.5 Å<sup>2</sup> vs. 31.1 Å<sup>2</sup>) rendering the conformation of the former less stable. This is possibly due to the already mentioned absence of a water molecule in **In-diff** that bridges Trp9 with the protein main chain in the **In** conformation.

The free energy surface from a 250 ns metadynamics simulation with the **In-diff** model (Supporting Information) shows that when the [Fe<sub>2</sub>S<sub>2</sub>] cluster is reduced, the Trp9 conformation observed in the H33A variant (here called **Wi'**) is still a minimum. However, there are protein conformations where Trp9 is solvent-exposed that are lower in energy (Figure S20a). Conversely, when the simulation is carried out with an oxidized [Fe<sub>2</sub>S<sub>2</sub>] cluster, the **Wi'** Trp9 conformation is no longer a minimum and several alternative minima for the Trp9 position are observed (Figure S20b). Besides confirming that the His-to-Ala substitution has destabilized this region by creating a larger cavity, these minima, which should easily switch to an out conformation, explain the extensive Trp9 modification observed in both redox states (Figure S16).

**pH dependence of DNA binding affinity of wild type and the H33A variant tested by EMSA.** The molecular dynamic simulations described above have generated a consistent reaction model for the redox-dependent modulation of DNA binding by SvRsrR. This model implies that the observed shift of His33 between the **Out** and **In** forms is caused by its protonation upon cluster reduction. One way to test this hypothesis experimentally is to monitor the DNA-binding affinity of the oxidized protein as a function of pH. Indeed, it may be anticipated

from the expected pKa values of His residues that at acidic pH His33 will be protonated even in the oxidized state. This, in turn, will cause it to shift toward the cluster, which still has an overall charge of -1, creating the cavity that allows Trp9 to adopt its **Wi** position in the **In** protein form. As shown by the SvRsrR-DNA complex structure this form cannot bind DNA. Conversely, the DNA-binding affinity of the H33A variant should not vary significantly as a function of pH if His33 plays a key role in that binding. We have tested this hypothesis by running EMSAs at pH 7.0, 6.0 and 5.0 for wild type and H33A SvRsrR (Figure 8). In accordance with our predictions, the oxidized wild type RsrR shows a marked drop in DNA-binding affinity at pH 5.0 relative to pH 7.0. Indeed, whereas a ratio of  $[\text{Fe}_2\text{S}_2]$  (corresponding to active dimeric protein) to DNA of about 1.0 was required to obtain 50% bound DNA at pH 7.0, at pH 5.0 that ratio was about 2.0. The corresponding values in the case of the H33A variant were 0.9 and 1.2. We verified that the pH changes did not significantly affect cluster integrity in either case (Figure S21).

These results clearly show that protonation of His33 has a direct negative effect on SvRsrR DNA binding affinity.

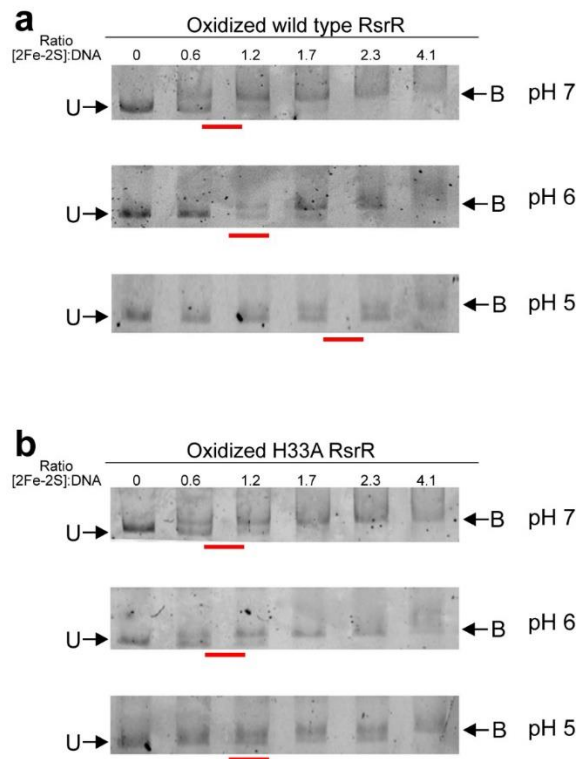


**Figure 8.** pH-dependent DNA binding of wild type and H33A variant determined by EMSA. Red bars indicate the ratio of  $[\text{Fe}_2\text{S}_2]$  RsrR to DNA required for 50% binding of DNA in each experiment. U = unbound, B = bound.

## DISCUSSION.

Several transcription regulators use iron-sulfur clusters as sensors of effectors such as NO, O<sub>2</sub>, oxidative stress, iron concentration and cell  $[\text{Fe-S}]$  cluster status. Sensing is generally mediated by the chemical modification of the cluster, including its partial or total disassembly which, in turn, determines regulator binding to specific DNA sites. In this respect, SvRsrR is

exceptional because its DNA-binding is modulated by the reversible one-electron oxidation of its  $[\text{Fe}_2\text{S}_2]$  cluster. The sensing of a single electron is consistent with the proposed role of SvRsrR in regulating the redox status of the cell. But it also poses a major challenge to elucidate the underlying mechanism. In our previous work, we determined that, in a crystal containing partially reduced SvRsrR, Trp9 could adopt two very distinct conformations, generating mixed protein dimers. These different conformations also modified the helix-turn-helix motif, suggesting that they were instrumental in modulating DNA binding. The fact that the tryptophan indole side chain has a dipole hinted at the possibility that its observed rotation was caused by changes in the local electrostatic field correlated with the redox state of the  $[\text{Fe}_2\text{S}_2]$  cluster. However, due to crystal packing effects, we could not assign a Trp9 conformation to a given redox state using only our SvRsrR crystals. We have now circumvented this problem by probing the extent of chemical modification of Trp9 in solution in the oxidized and reduced states. This experiment has shown unambiguously that the solvent-exposed Trp9 in the **Out** conformation (**Wo**) corresponds to the oxidized 2+  $[\text{Fe}_2\text{S}_2]$  cluster and the buried Trp9 in the **In** conformation (**Wi**) corresponds to the reduced 1+ species. Furthermore, using the molecular replacement method, we have shown that *only* the **Out** protein conformation (Figure 1b, in green) provides a correct solution for the medium-resolution crystal structure of a SvRsrR-DNA complex, which is only stable in solution when the SvRsrR  $[\text{Fe}_2\text{S}_2]$  is in the oxidized state. By combining X-ray data from two different complex structures we have obtained a model where the crucial Trp9 and His33 residues have well defined electron density. A comparison of the SvRsrR **Out** uncomplexed form with the complexed one shows they significantly differ at the positions of these two residues and that of Tyr39, which establishes an H-bond with the DNA fragment. Furthermore, a superposition of the **In** form onto the complexed SvRsrR reveals severe clashes of the former with the DNA fragment. This observation explains why the **In** form cannot bind the nucleic acid.

We next focused our interest on the imidazole ring of His33, which also changes orientation between the **Out** (oxidized) and **In** (reduced) conformations (Figure 1b). Because His33 sits closer to the  $[\text{Fe}_2\text{S}_2]$  cluster in the reduced SvRsrR structure, we reasoned that it could be protonated in that state. Molecular dynamics simulations clearly showed that only the **Out/Ox/H33<sup>0</sup>** and **In/Red/H33<sup>+</sup>** states were consistent with the **Out** and **In** SvRsrR crystal structures, respectively (Figures 4 and 5). Furthermore, a metadynamics simulation starting from the hypothetical **Out/Red/H33<sup>+</sup>** state, modeled from the **Out** crystal structure by the addition of one proton and one electron, is the only ‘proton/electron’ configuration that nicely leads to a structure very close to the **In** state; this includes the migration and bonding of a buried water molecule (Figures 6b and S9). Moreover, inspection of electrostatic effects shows that protonation of His33 lowers the rotational barrier of the Trp9 side chain between **Wo** and **Wi** (Figure 7b). Along with other associated interactions, this makes the Trp9 rotation favorable.

Our calculations also suggest that the displacement of the positively-charged imidazole ring caused by electrostatic attraction resulting from  $[\text{Fe}_2\text{S}_2]$  cluster reduction (Figure 1b) is energetically favorable, even though it requires the breaking of the hydrogen bond between the N $\delta$ 1 of His33 and the carbonyl oxygen of Leu29 (Figure 4c). This bond breaking is essential to generate **In/Red/H33<sup>+</sup>** (Figure 5c), which, in turn, opens up an

internal cavity into which water molecules can diffuse and Trp9 rotate.

The proposed protonation of His33 requires a change in  $pK_a$  of its N $\epsilon$ 2 atom in the reduced *SvRsrR* towards a more basic value than the one expected in water, which is  $\sim 6.0$ . Very significant  $pK_a$  changes upon reduction have been both observed and calculated for the two  $[\text{Fe}_2\text{S}_2]$  cluster His ligands of Rieske-type proteins. Indeed, these ligands are bound to the same Fe ion and their  $pK_a$  values change from 7.4/9.1 in the oxidized protein up to 12.6 in the reduced one.<sup>18</sup> This change to much more basic values results from the  $[\text{Fe}_2\text{S}_2]$  cluster reductive electron delocalizing to the bound imidazole ring. A similar effect is expected on the His12 cluster ligand of *SvRsrR*. Conversely, His33 is not bound to the  $[\text{Fe}_2\text{S}_2]$  cluster and the reduction of the latter should have a lesser effect on its  $pK_a$ . Nevertheless, in the High Potential Iron-Sulfur Protein (HiPiP) from *Chromatium vinosum*,  $pK_a$  values of 6.7 and 7.3 have been reported for its His42 in the oxidized and reduced states, respectively.<sup>19</sup> The nearest atom of the His42 imidazole ring is located about 9 Å away from the  $[\text{Fe}_4\text{S}_4]$  HiPiP cluster, a distance that is  $\sim 1$  Å further away than His33 is from the *SvRsrR*  $[\text{Fe}_2\text{S}_2]$  cluster.

At this point we do not know the extent to which the  $pK_a$  of His33 is affected by the redox state of the cluster. However, even if the change was small, the observation that His residues typically have  $pK_a$  values close to neutrality should favor its acid-base transition. If His33 responds to electrostatic changes, its N $\epsilon$ 2 would be protonated when the cluster is reduced and

deprotonated when it is oxidized (the N $\delta$ 1 atom should be always protonated as it forms a hydrogen bond to a carbonyl oxygen in both states; Figure 9a). A  $pK_a$  shift to more basic values upon reduction is hinted at by quantum mechanical calculations that show the molecular orbital rearrangement upon  $[\text{Fe}_2\text{S}_2]$  cluster reduction (Figure S10), lowering the His33 orbital down to the frontier orbital region. The orbital rearrangement increases the probability that the reducing electron - which is localized at the Fe atom bound to His12 (Supporting Information) - will thermally leak towards His33 thus favoring its protonation and its subsequent shift in the cluster's direction.

In our previous work, we investigated the unprecedented cluster ligation (Glu8, His12, Cys90 and Cys110).<sup>9</sup> Replacing Glu8 and His12 with cysteine residues maintains the integrity of the  $[\text{Fe}_2\text{S}_2]$  cluster but it becomes unstable to redox cycling and DNA binding is impaired. We argued at the time that the natural choice of Glu and His may be linked to stereochemical constraints. Indeed, the different residue lengths of Glu and His versus that of Cys determine the position of N-terminal residues Gly5, Gly6 and Trp9 close to or at the DNA-binding site. This is now confirmed by the structure of the DNA complex. We can now add the fact that a four-cysteine ligation will delocalize the reducing electron onto both iron sites, thus pulling some electron density away from the His12-coordinated Fe atom and breaking the directionality towards His33 via His12.

The substitution of His33 by Ala disrupts this mechanism and the cavity observed in the wild type protein, where a water molecule and Trp9 are found in the **In** form (Figure 5c), is therefore not generated in the H33A variant.

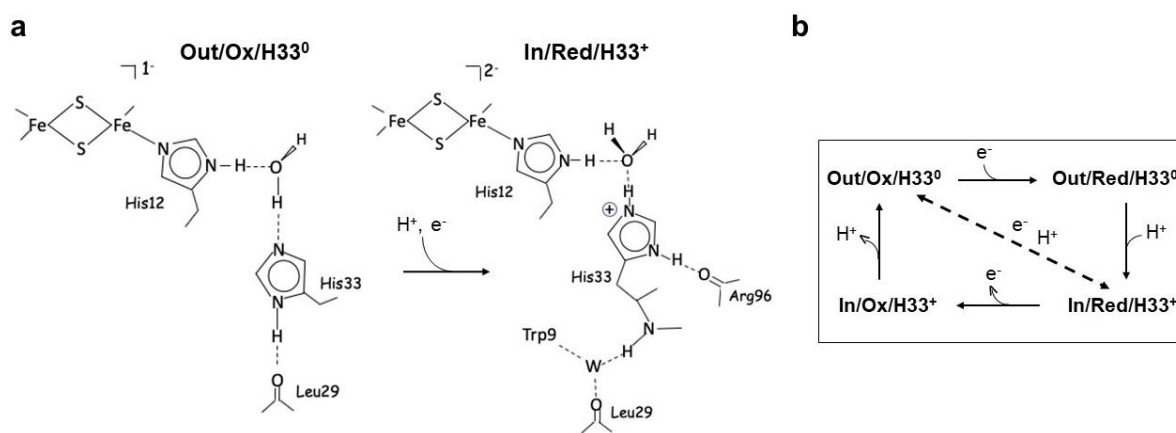


**Figure 9.** Proposed *SvRsrR* redox-dependent mechanism of DNA binding by *SvRsrR*. **a** Conformational changes required in going from **Out/Ox/H33<sup>0</sup>** to **In/Red/H33<sup>+</sup>**. **b** Proposed sequential cyclic redox and protonation/deprotonation events (solid arrows). The dashed arrow indicates a concerted proton-coupled electron transfer (PCET) process.

Packing analysis of the different crystals shows that a loop from the *SvRsrR* helix-turn-helix motif is remarkably flexible, a probably inherent conformational property that facilitates the **Out**-to-**In** transition. Indeed, in the H33A-*SvRsrR* variant crystal the flexibility of this loop allows the formation of a cavity that is partially occupied by Trp9 in its **In-diff** form (Figure S19). However, the crystal structure also indicates that in this variant Trp9 cannot adopt the stabilized **In** position found in the wild type reduced protein. This, in turn, explains why, as shown by the electrophoretic mobility shift assays, H33A-*SvRsrR* can display the DNA-binding **Out-like** conformation in both the oxidized and the reduced state of its  $[\text{Fe}_2\text{S}_2]$  cluster. Hence, these

results show that His33 plays a fundamental role in the **Out** to **In** transition and in the redox-dependent modulation of *SvRsrR* DNA binding.

According to our results, His33 protonation should play a fundamental role in DNA-binding modulation. Thus, we sought to provide experimental evidence for it, through a series of EMSAs with oxidized wild type and His33A-*SvRsrR* as a function of pH. We find that at pH 5.0 the DNA-binding affinity of the wild type protein is significantly lower than that observed at pH 7.0. The same experiment performed with the H33A variant shows a comparatively minor drop in affinity over the same pH range. We conclude from these results that protonation of His33

favors the **In** conformation, even when SvRsrR is oxidized causing the shift of this residue towards the cluster mimicking what takes place in the reduced protein.

Figure 9 summarizes the electron and proton transfers determined here to be essential for the redox-dependent mechanism of DNA binding of SvRsrR. These transfers can be either sequential or concerted depending on whether or not intermediate states are stable enough to be characterized<sup>20</sup>. In the case of SvRsrR, the pK<sub>a</sub> change of His33, expected to occur upon reduction, appears to be essential for its protonation; this, in turn, suggests that reduction is followed by protonation, and oxidation by deprotonation, starting from the top left in Figure 9b. The alternative proton-coupled electron transfer, PCET (dashed diagonal arrow in this Figure) would require the simultaneous reduction of the [Fe<sub>2</sub>S<sub>2</sub>] cluster and protonation of His33, which is more difficult to explain in electrostatic terms. Furthermore, our pH-dependent EMSA experiments strongly suggest that His33 protonation can take place in the absence of reduction and, consequently, the two processes do not have to be coupled. Implicit in Figure 9a is the fact that the redox process affecting the [Fe<sub>2</sub>S<sub>2</sub>] cluster is necessary for the **Out**-to-**In** conformational change of Trp9. The original idea that the orientation of the indole dipole was mainly determined by the SvRsrR [Fe<sub>2</sub>S<sub>2</sub>] cluster redox state has now been expanded to consider all the charges that contribute to the electric field present at the cavity occupied by Trp9 in the **In** conformation. Our main conclusion is that, although the Trp9 indole dipole plays an essential role in determining the stability of this form, there is a complex interplay between [Fe<sub>2</sub>S<sub>2</sub>] cluster reduction, His33 protonation and the overall protein structure that determines the value of the rotation barrier for Trp9 between the **In** and **Out** conformations. In summary, SvRsrR uses both one-electron reduction and a single protonation to elicit a complex series of events that lead to the creation of an internal cavity that is occupied by a water molecule and the burial of Trp9 close to it. This process is facilitated by changes in the electric field. The crucial role played by the proton that accompanies SvRsrR cluster reduction may represent a novel strategy in sequential electron and proton transfer processes. The combination of these effects leads to conformational changes that are sufficiently dramatic to promote or abolish protein-DNA binding interactions.

## METHODS

**Purification of variant SvRsrR proteins.** Plasmids for the preparation of W123F/W154F and H33A site-directed variant of C-terminally His-tagged SvRsrR were purchased from Genscript. Proteins were purified as previously described using the same procedure as for wild type SvRsrR.<sup>5,9</sup> SvRsrR protein concentrations were determined using the method of Bradford (Bio-Rad Laboratories), with BSA as the standard.<sup>21</sup> Cluster concentrations were determined using  $\epsilon_{455\text{ nm}} = 3450 \pm 25 \text{ M}^{-1} \text{ cm}^{-1}$  for the oxidized form<sup>5,9</sup>. Cluster loadings were as follows: Wild type SvRsrR, 80%; W123F/W154F, 74%; H33A, 70%. SvRsrR [Fe<sub>2</sub>S<sub>2</sub>] clusters were oxidized by exposure to atmospheric O<sub>2</sub> and incubation for 10–30 min. Reduction was achieved through the addition of a 6-fold excess of sodium dithionite. Reduction occurred immediately though, in some cases, samples were incubated prior to spectral measurement. Variant proteins behaved as the wild type protein in that oxidized and reduced forms were entirely stable and could be redox cycled numerous times without significant cluster loss or protein precipitation.

**RsrR residue side chain solvent accessibility experiments.** A solution of ammonium acetate (250 mM, pH 7.5) was saturated

with chloroform (29  $\mu\text{l/ml}$ ) and used for the preparation of a solution of as isolated SvRsrR (~100  $\mu\text{M}$  cluster) containing a reduced [Fe<sub>2</sub>S<sub>2</sub>] cluster. Any precipitated material was removed by centrifugation and the CD spectrum recorded. The sample was then irradiated for 60 min using a 450 W Xe lamp (Jasco J-810 spectropolarimeter) at 280 nm (10 nm slit width) in a cylindrical 1 cm quartz cuvette.<sup>15</sup> After irradiation, any precipitated material was again removed by centrifugation and the CD spectrum recorded again. An aliquot (50  $\mu\text{l}$ ) was then removed for LC-MS analysis. The same procedure was repeated for oxidized SvRsrR, prepared by exposure to atmospheric O<sub>2</sub> and incubation for 10–30 min.<sup>5,9</sup>

**Liquid chromatography mass spectroscopy (LC-MS).** LC-MS samples were diluted (to ~10  $\mu\text{M}$ ) with an aqueous mixture of 2% (v/v) acetonitrile, 0.1% (v/v) formic acid in an LC-MS vial. LC-MS samples were removed from the anaerobic cabinet and loaded onto a ProSwift RP-1S column (4.6  $\times$  50 mm) (Thermo Scientific) using an Ultimate 3000 uHPLC system (Dionex, Leeds, UK). Bound proteins were eluted (0.2 ml/min) using a linear gradient (15 min) from 2% to 100% (v/v) acetonitrile, 0.1% (v/v) formic acid. The eluent was continuously infused into a Bruker microQTOF-QIII mass spectrometer, running Hystar (Bruker Daltonics, Coventry, UK), using positive mode electrospray ionisation (ESI). Compass Data Analysis 4.1 with Maximum Entropy v1.3 was used for processing of spectra under the LC peak. The mass spectrometer was calibrated with ESI-L tuning mix (Agilent Technologies, California, USA). Mass spectrometry data are presented in terms of relative abundance, with the most abundance peak assigned to 100% and all other peaks reported relative to it (% relative abundance).

**MS/MS Analysis.** An aliquot (250  $\mu\text{l}$ ) of the protein was chloroform-methanol precipitated and centrifuged at 17,000  $\times$  g for 5 min at an ambient temperature.<sup>22</sup> The upper aqueous methanol layer was removed, 500  $\mu\text{l}$  of methanol added, gently mixed by inversion, and centrifuged as above. The supernatant was removed, and the pellet dried at 37 °C for ~30 min. Digestion was carried out using a Proteoextract All-in-one Trypsin digestion kit (Calbiochem), following the manufacturer's *in-solution* protocol. The resulting samples were diluted to 250  $\mu\text{l}$  with 2% (v/v) acetonitrile 0.1% formic acid and an aliquot (10  $\mu\text{l}$ ) of the sample was injected onto a Kinetex Evo C18 column (100 Å, 2.6 mm, 150  $\times$  2.1 mm, Phenomenex) via an Ultimate 3000 uHPLC systems (Dionex, Leeds, UK). Peptides were eluted (0.2 ml/min) by increasing acetonitrile from 2% to 10% (v/v) immediately after sample injection and holding for 5 min, and then applying a linear gradient between 10 and 100% acetonitrile, 0.1% formic acid over 75 min. The eluant was continuously infused into a Bruker microQTOF-QIII mass spectrometer using positive ion mode electrospray ionisation (ESI). Acquisition was controlled by Bruker oTOF Control software with the following parameters: dry gas flow of 8 L/min, nebulizer gas pressure of 0.8 Bar, dry gas at 200 °C, capillary voltage of 4,500 V, offset of 500 V, ion energy of 3 eV. Nitrogen served as the carrier and collision gas. Ions  $\geq 307 \text{ m/z}$  and  $\geq 1000$  counts in intensity were selected for auto CID fragmentation, during which the collision energy was swept between 70–275% (~25 to 128 eV) of default values. Bruker Smart exclusion was employed to reduce the selection background ions. HPLC and MS functions were integrated by HyStar (Bruker Daltonics, Coventry, UK). Before processing, data sets were re-calibrated off-line with sodium formate. Compass Data Analysis 4.1, BioTools and Sequence Editor v3.2 (Bruker Daltonics, Coventry, UK) were used for data processing.

**Electrophoretic mobility shift assays (EMSAs).** EMSA reactions (20  $\mu\text{l}$ ) were carried out on ice in 10 mM Tris, 60 mM KCl, pH 7.52, as previously described. Probe DNA was the 5' 6-FAM-labelled intergenic region between *S. venezuelae* *sven1847* and *sven1848*.<sup>5,9</sup> Briefly, varying amounts of wild type or variant SvRsrR protein were added to 1  $\mu\text{L}$  of DNA, followed by 2  $\mu\text{L}$  of

loading dye (containing 0.01% (w/v) bromophenol blue). Reaction mixtures were immediately separated at 30 mA on a 5% (w/v) polyacrylamide gel in 1 x TBE (89 mM Tris, 89 mM boric acid, 2 mM EDTA), using a Mini Protean III system (Bio-Rad). Polyacrylamide gels were pre-run at 30 mA for 2 min prior to use. A GE Healthcare Typhoon FLA-9500 was used to visualize gels (excitation, 473 nm; emission, 510 nm).

Oxidized W123F/W154F exhibited binding to a SvRsrR-regulated DNA sequence that was very similar to that of the wild type protein (Figures S1b and S2b), while the reduced form exhibited little propensity to bind DNA, as also observed for wild type SvRsrR.<sup>5</sup> Thus, the conformational switch that modulates DNA-binding in response to the redox state of the cluster is entirely preserved in this variant. A markedly different result was obtained with the H33A variant that displayed DNA binding in both the oxidized and reduced states (Figure S16).

To investigate the effect of pH, EMSA reactions were prepared with wild type or H33A SvRsrR in binding buffers of varying pH: Tris (10 mM Tris 2.5% glycerol) at pH 7; and Bis-tris propane (10 mM Bis-tris-propane, 2.5% glycerol) at pH 6 and pH 5. Polyacrylamide gels were prepared with Bis-tris (19 mM Bis-tris, pH 7), HEPES (37 mM HEPES, pH 6) or MES (37 mM MES, pH 5) buffer containing 1.5 mM EDTA.<sup>23</sup> Reaction mixtures were immediately separated at 30 mA for 15 min.

**Optical spectroscopy.** To investigate the effect of pH on cluster integrity, an aliquot of oxidized wild type or H33A SvRsrR was prepared in 10x Tris (pH 8, 7.5 and 7) or Bis-tris-propane (pH 6 and pH 5) EMSA binding buffers to ~300  $\mu$ M [Fe<sub>2</sub>S<sub>2</sub>] and UV-visible absorbance and CD spectra recorded. We note that CD spectra in 100 mM Tris, 25% glycerol pH 8 was better resolved than that recorded in 50 mM Tris, 2 M NaCl, 5% glycerol, pH 8 (Figure S21).

**Crystallization experiments.** Crystals of SvRsrR complexed with DNA were obtained as follows. A solution of 18 mg/mL of SvRsrR was incubated for 90 minutes at room temperature under air with a fourfold excess of a double-stranded non-palindromic 39 base-pair (bp) DNA fragment (Figure 3a) in 300 mM NaCl, 50 mM Tris and 5% glycerol at pH 8.0. The resulting complex was transferred to an anaerobic glovebox and crystallization conditions from commercial kits were set up in 96-well plates using the vapor diffusion method with a Gryphon robot (Art Robbins Instruments, CA, USA). The crystallization drops were prepared by mixing 300 nL of the complex solution with 100 nL of the commercial solution and equilibrated with 100  $\mu$ L of the latter at 20°C. Crystals grew from a solution consisting of 12.5% methyl-pentanediol, 12.5% PEG1000, 12.5% PEG3350, 55.5 mM MES pH 6.5, 44.5 mM imidazole, 30 mM MgCl<sub>2</sub> and 30 mM CaCl<sub>2</sub>. After two weeks, the best-looking crystal was transferred to a cryo-protecting solution consisting of 12% methyl-pentanediol, 12% PEG1000, 12% PEG3350, 55.5 mM MES pH 6.5, 44.5 mM imidazole, 30 mM MgCl<sub>2</sub> and 30 mM CaCl<sub>2</sub>, supplemented with 15% glycerol. This crystal (number 2 in Table S1) was then mounted in a cryo-loop and flash-cooled in liquid propane inside the glovebox<sup>24</sup> before being stored in liquid nitrogen. The same protein-DNA complex (prepared with a 1:4 protein to DNA ratio), exposed to air for 60 min before being transferred to the glovebox, was used to set up hanging drops in a Limbro plate in the glove box at room temperature. The drops were prepared by mixing 2  $\mu$ L of the complex solution and 1  $\mu$ L of a crystallization solution consisting of 15% methyl-pentanediol, 15% PEG1000, 15% PEG3350, 41.3 mM MES pH 7.0, 58.7 mM imidazole, 30 mM MgCl<sub>2</sub> and 30 mM CaCl<sub>2</sub>, and equilibrated with 1 mL of the latter solution. Nine months later, a crystal grown under these conditions (number 1 in Table S1) was mounted in a cryo-loop and stabilized in a cryo-protecting solution consisting of 18% methyl-pentanediol, 18% PEG1000, 18% PEG3350, 41.3 mM MES pH 7.0, 58.7 mM imidazole, 30 mM

MgCl<sub>2</sub>, 30 mM CaCl<sub>2</sub> and 15% glycerol, flash-cooled in liquid propane and stored in liquid nitrogen.

The as-isolated SvRsrR H33A variant was crystallized anaerobically from drops obtained by mixing 1  $\mu$ L of 18 mg/ml of protein in 300 mM NaCl, 5% (v/v) glycerol and 50 mM Tris pH 8.0 with 1  $\mu$ L of 50-55% (v/v) methyl-pentanediol, 100 mM MES pH 6.0, 2 mM dithionite. The drop was then equilibrated against 1000  $\mu$ L of the latter at 20 °C. A pink plate-like crystal obtained under these conditions after 3 weeks was transferred to a cryo-protecting solution composed of 80% (v/v) methyl-pentanediol, 100 mM MES pH 6.0, 2 mM dithionite, mounted in a cryo-loop and flash-cooled in liquid propane inside the glovebox.

**X-ray data collection and structure determination.** SvRsrR-DNA complex: Anisotropic X-ray diffraction data were first collected from complex 2 to a resolution of 4.1 Å (Table S1) at beamline ID30-A3 of the European Synchrotron Radiation Facility in Grenoble, France. For complex 1 nearly isotropic X-ray diffraction data to 4.3 Å resolution (Table S1) were measured later at beamline PXI of the Swiss Light Source (Villigen, Switzerland). The two datasets were indexed and integrated with the *XDS* package<sup>25</sup> and scaled with *AIMLESS*.<sup>26</sup> Complex 2 has pseudo-orthorhombic symmetry and is about 50% twinned according to a statistical analysis of its X-ray intensities. Conversely, no twinning was detected for the hexagonal complex 1 crystal which was therefore chosen for the initial phasing by molecular replacement with *PHASER*<sup>27</sup> (for details see Supporting Information). The obtained structure was then used to get a good starting model for complex 2. Subsequent electron density averaging between the two crystals greatly improved the maps. Satisfactory refinement statistics were obtained for both complexes (Table S3) after rigid body refinement and application of non-crystallographic symmetry (ncs) restraints for positional refinement with *PHENIX*<sup>28</sup> and *REFMAC5*.<sup>29</sup> In addition, the 1.6 Å resolution structure of the oxidized form of the SvRsrR dimer (pdb code 6HSD) was used as a reference model. Application of hydrogen bond restraints for DNA base pairs and non-bonded distance restraints for stacked DNA bases and for the [Fe<sub>2</sub>S<sub>2</sub>] cluster was essential to keep their stereochemistry within reasonable values and greatly improved the refinement statistics (Table S3). All manual model corrections were performed with *COOT*.<sup>30</sup> Given the limited resolution of 4.3 Å, refinement of thermal parameters was restricted to only grouped B-factors with *PHENIX*. Finally, for complex 1 strongly damped refinement cycles of atomic positions and isotropic B-factors, without ncs restraints, were performed with *REFMAC5*. Starting from that model, complex 2 was refined with *PHENIX* (atomic positions and grouped B-factors only) without any manual model corrections (Table S3).

H33A-SvRsrR: X-ray diffraction data to 1.68 Å resolution were collected for this variant (Table S1) at beamline PX-2A of the SOLEIL synchrotron in Saclay, France. The structure solution was performed with programs also used for the SvRsrR-DNA complex, i.e. *XDS* for data indexing and integration, *AIMLESS* for scaling, *PHASER* for phasing by molecular replacement, *PHENIX* and *REFMAC* for refinement of rigid bodies, atomic positions and isotropic B-factors and *COOT* for manual model corrections. Individual anisotropic B-factors were refined in the final step. Refinement statistics are given in Table S3.

**Calculations.** Except for the electrostatic energy profiles, the Schrödinger suite<sup>31</sup> was used for calculations (See Supporting Information for details). Electrostatic potential (ESP) charge calculations were performed with the Jaguar quantum chemistry program<sup>32</sup> while the QSite program,<sup>33</sup> which combines quantum and molecular mechanics (QM/MM), was employed to analyze the effect of cluster reduction on His33; subsequent orbital analysis was done within the Maestro graphics interface of the Schrödinger suite.<sup>31</sup> Desmond<sup>34</sup> was used for all MD and metadynamics simulations.

All electrostatic energy profiles were calculated with a Fortran code written by JMM using either the **Out** or the **In** atomic coordinates of the [Fe<sub>2</sub>S<sub>2</sub>] cluster and its four ligands, His33 and Trp9, their atomic charges derived by QM calculations, and point charges of the surrounding charged residues (See Supporting Information for details).

## ASSOCIATED CONTENT

### Supporting Information.

This material is available free of charge via the Internet at <http://pubs.acs.org>.

Additional experimental and calculations details, supporting figures and tables (PDF).

## AUTHOR INFORMATION

### Corresponding Author

\* [N.Le-brun@uea.ac.uk](mailto:N.Le-brun@uea.ac.uk), [juan.fontecilla@ibs.fr](mailto:juan.fontecilla@ibs.fr)

### Present Addresses

<sup>‡</sup> Current address: Centro de Biotecnología y Genómica de Plantas (CBGP), Universidad Politécnica de Madrid (UPM), Instituto Nacional de Investigación y Tecnología Agraria y Alimentaria (INIA), Madrid, Spain.

### Author Contributions

The manuscript was written through contributions of all authors. All authors have given approval to the final version of the manuscript.

<sup>§</sup> These authors contributed equally.

### Funding Sources

This work was partially supported by the MANGO-ICING contract from the Agence Nationale pour la Recherche (ANR-18-CE11-0010) and by FRISBI (ANR-10-INSB-05-02) within the Grenoble Partnership for Structural Biology (PSB). This work was also supported by the Biotechnology and Biological Sciences Research Council through grant BB/P006140/1, by UEA through the award of a PhD studentship to MTPM and purchase of the ESI-MS instrument, and by the FeSBioNet COST Action CA15133. Parts of the research leading to these results has received funding from the European Union's Horizon 2020 research and innovation program under grant agreement n° 730872, project CALIPSOplus.

### Notes

The atomic coordinates and structure factors will be deposited in the Protein Data Bank, (PDB ID codes XXX and YYY for the SvRsrR-DNA complex and the H33A-SvRsrR variant, respectively).

## ACKNOWLEDGMENT

P.A. thank Drs David Rinaldo and Davide Branduardi from Schrödinger LLC and appreciate the help from the staff of the computing facility provided by the Commissariat à l'Energie Atomique (CEA/DSV/GIPSI), Saclay, and (CCRT), Bruyères-le-Châtel. The authors are also very grateful to Pierre Legrand for X-ray data collection and initial structure solution of the RsrR H33A variant at the PROXIMA-2 beam line of the SOLEIL synchrotron (Saclay, France). We thank Thomas McClean and Prof Matthew Hutchings (School of Biological Sciences, UEA) for assistance with EMSAs and general discussions.

## REFERENCES

- (1) Shepard, W.; Soutourina, O.; Courtois, E.; England, P.; Haouz, A.; Martin-Verstraete, I. Insights into the Rrf2 Repressor Family -the Structure of CymR, the Global Cysteine Regulator of *Bacillus Subtilis*. *FEBS J.* **2011**, *278* (15), 2689–2701.
- (2) Santos, J. A.; Pereira, P. J. B.; Macedo-Ribeiro, S. What a Difference a Cluster Makes: The Multifaceted Roles of IscR in Gene Regulation and DNA Recognition. *Biochim. Biophys. Acta, Proteins Proteomics* **2015**, *1854* (9), 1101–1112.
- (3) Hibbing, M. E.; Fuqua, C. Antiparallel and Interlinked Control of Cellular Iron Levels by the Irr and RirA Regulators of *Agrobacterium Tumefaciens*. *J. Bacteriol.* **2011**, *193* (14), 3461–3472.
- (4) Crack, J. C.; Munnoch, J.; Dodd, E. L.; Knowles, F.; Al Basam, M. M.; Kamali, S.; Holland, A. A.; Cramer, S. P.; Hamilton, C. J.; Johnson, M. K.; et al. NsrR from *Streptomyces Coelicolor* Is a Nitric Oxide-Sensing [4Fe-4S] Cluster Protein with a Specialized Regulatory Function. *J. Biol. Chem.* **2015**, *290* (20), 12689–12704.
- (5) Munnoch, J. T.; Martinez, M. T. P.; Svistunenko, D. A.; Crack, J. C.; Le Brun, N. E.; Hutchings, M. I. Characterization of a Putative NsrR Homologue in *Streptomyces Venezuelae* Reveals a New Member of the Rrf2 Superfamily. *Sci. Rep.* **2016**, *6*, 31597.
- (6) Fleischhacker, A. S.; Stubna, A.; Hsueh, K.-L.; Guo, Y.; Teter, S. J.; Rose, J. C.; Brunold, T. C.; Markley, J. L.; Münck, E.; Kiley, P. J. Characterization of the [2Fe-2S] Cluster of *Escherichia Coli* Transcription Factor IscR. *Biochemistry* **2012**, *51* (22), 4453–4462.
- (7) Martinez, M. T. P.; Martinez, A. B.; Crack, J. C.; Holmes, J. D.; Svistunenko, D. A.; Johnston, A. W. B.; Cheesman, M. R.; Todd, J. D.; Brun, N. E. L. Sensing Iron Availability via the Fragile [4Fe-4S] Cluster of the Bacterial Transcriptional Repressor RirA. *Chem. Sci.* **2017**, *8* (12), 8451–8463.
- (8) Volbeda, A.; Dodd, E. L.; Darnault, C.; Crack, J. C.; Renoux, O.; Hutchings, M. I.; Le Brun, N. E.; Fontecilla-Camps, J. C. Crystal Structures of the NO Sensor NsrR Reveal How Its Iron-Sulfur Cluster Modulates DNA Binding. *Nat. Commun.* **2017**, *8*, 15052.
- (9) Volbeda, A.; Martinez, M. T. P.; Crack, J. C.; Amara, P.; Gigarel, O.; Munnoch, J. T.; Hutchings, M. I.; Darnault, C.; Le Brun, N. E.; Fontecilla-Camps, J. C. Crystal Structure of the Transcription Regulator RsrR Reveals a [2Fe-2S] Cluster Coordinated by Cys, Glu, and His Residues. *J. Am. Chem. Soc.* **2019**, *141* (6), 2367–2375.
- (10) Rajagopalan, S.; Teter, S. J.; Zwart, P. H.; Brennan, R. G.; Phillips, K. J.; Kiley, P. J. Studies of IscR Reveal a Unique Mechanism for Metal-Dependent Regulation of DNA Binding Specificity. *Nat. Struct. Mol. Biol.* **2013**, *20* (6), 740–747.
- (11) Santos, J. A.; Alonso-García, N.; Macedo-Ribeiro, S.; Pereira, P. J. B. The Unique Regulation of Iron-Sulfur Cluster Biogenesis in a Gram-Positive Bacterium. *Proc. Natl. Acad. Sci. U.S.A.* **2014**, *111* (22), E2251–2260.
- (12) Newton, G. L.; Buchmeier, N.; Fahey, R. C. Biosynthesis and Functions of Mycothiol, the Unique Protective Thiol of Actinobacteria. *Microbiol. Mol. Biol. Rev.* **2008**, *72* (3), 471–494.
- (13) Edwards, R. A.; Jickling, G.; Turner, R. J. The Light-Induced Reactions of Tryptophan with Halocompounds. *Photochem. Photobiol.* **2002**, *75* (4), 362–368.
- (14) Vorobey, A.; Chernitsky, E.; Konev, S.; Krivitsky, A.; Pinchuk, S.; Shukanova, N. Chloroform-Dependent Photoproducts of Tryptophan. *Biofizika* **1992**, *37* (5), 848–850.
- (15) Ladner, C. L.; Turner, R. J.; Edwards, R. A. Development of Indole Chemistry to Label Tryptophan Residues in Protein for Determination of Tryptophan Surface Accessibility. *Protein Sci.* **2007**, *16* (6), 1204–1213.
- (16) Barducci, A.; Bonomi, M.; Parinello, M. Metadynamics. *WIREs Comput. Mol. Sci.* **2011**, *1*, 826–843.
- (17) Bussi, G.; Branduardi, D. Free-Energy Calculations with Metadynamics. In *Reviews in Computational Chemistry*;

- Abby L. Parrill, Kenny B. Lipkowitz: New York, 2015; Vol. 28.
- (18) Hsueh, K.-L.; Westler, W. M.; Markley, J. L. NMR Investigations of the Rieske Protein from *Thermus Thermophilus* Support a Coupled Proton and Electron Transfer Mechanism. *J. Am. Chem. Soc.* **2010**, *132* (23), 7908–7918.
- (19) Nettesheim, D. G.; Meyer, T. E.; Feinberg, B. A.; Otvos, J. D. Comparative Nuclear Magnetic Resonance Studies of High Potential Iron-Sulfur Proteins from *Chromatium Vinosum* and *Rhodospseudomonas Gelatinosa*. Additional Hyperfine Shifted Resonances and PH-Dependent Structural Perturbations. *J. Biol. Chem.* **1983**, *258* (13), 8235–8239.
- (20) Hammes-Schiffer, S. Proton-Coupled Electron Transfer: Moving Together and Charging Forward. *J. Am. Chem. Soc.* **2015**, *137* (28), 8860–8871.
- (21) Bradford, M. Rapid and Sensitive Method for Quantitation of Microgram Quantities of Protein Utilizing Principle of Protein-Dye Binding. *Analytical Biochem.* **1976**, *72* (1–2), 248–254.
- (22) Friedman, D. B. Quantitative Proteomics for Two-Dimensional Gels Using Difference Gel Electrophoresis. *Methods Mol. Biol.* **2007**, *367*, 219–239.
- (23) Deochand, D. K.; Perera, I. C.; Crochet, R. B.; Gilbert, N. C.; Newcomer, M. E.; Grove, A. Histidine Switch Controlling PH-Dependent Protein Folding and DNA Binding in a Transcription Factor at the Core of Synthetic Network Devices. *Mol. Biosyst.* **2016**, *12* (8), 2417–2426.
- (24) Vernede, X.; Fontecilla-Camps, J. C. A Method to Stabilize Reduced and or Gas-Treated Protein Crystals by Flash-Cooling under a Controlled Atmosphere. *J. Appl. Crystallogr.* **1999**, *32*, 505–509.
- (25) Kabsch, W. XDS. *Acta Crystallogr. D Biol. Crystallogr.* **2010**, *66* (Pt 2), 125–132.
- (26) Evans, P. R.; Murshudov, G. N. How Good Are My Data and What Is the Resolution? *Acta Crystallogr. D Biol. Crystallogr.* **2013**, *69* (Pt 7), 1204–1214.
- (27) McCoy, A. J.; Grosse-Kunstleve, R. W.; Adams, P. D.; Winn, M. D.; Storoni, L. C.; Read, R. J. Phaser Crystallographic Software. *J Appl Crystallogr* **2007**, *40* (Pt 4), 658–674.
- (28) Adams, P. D.; Afonine, P. V.; Bunkoczi, G.; Chen, V. B.; Davis, I. W.; Echols, N.; Headd, J. J.; Hung, L.-W.; Kapral, G. J.; Grosse-Kunstleve, R. W.; et al. PHENIX: A Comprehensive Python-Based System for Macromolecular Structure Solution. *Acta Crystallogr. Sect. D-Struct. Biol.* **2010**, *66*, 213–221.
- (29) Murshudov, G. N.; Skubák, P.; Lebedev, A. A.; Pannu, N. S.; Steiner, R. A.; Nicholls, R. A.; Winn, M. D.; Long, F.; Vagin, A. A. REFMAC5 for the Refinement of Macromolecular Crystal Structures. *Acta Crystallogr. D Biol. Crystallogr.* **2011**, *67* (Pt 4), 355–367.
- (30) Emsley, P.; Lohkamp, B.; Scott, W. G.; Cowtan, K. Features and Development of Coot. *Acta Crystallogr. D Biol. Crystallogr.* **2010**, *66* (Pt 4), 486–501.
- (31) Schrödinger Release 2018-3: Schrödinger, LLC, New York, NY, 2018.
- (32) Bochevarov, A. D.; Harder, E.; Hughes, T. F.; Greenwood, J. R.; Braden, D. A.; Philipp, D. M.; Rinaldo, D.; Halls, M. D.; Zhang, J.; Friesner, R. A. Jaguar: A High-Performance Quantum Chemistry Software Program with Strengths in Life and Materials Sciences. *Int. J. Quantum Chem.* **2013**, *113*, 2110–2142.
- (33) Murphy, R. B.; Philipp, D. M.; Friesner, R. A. A Mixed Quantum Mechanics/Molecular Mechanics (QM/MM) Method for Large-Scale Modeling of Chemistry in Protein Environments. *J. Comp. Chem.* **2000**, *21*, 1442–1457.
- (34) Bowers, K. J.; Chow, E.; Xu, H.; Dror, R. O.; Eastwood, M. P.; Gregersen, B. A.; Klepeis, J. L.; Kolossvary, M. A.; Sacerdoti, F. D.; Salmon, J. K.; et al. Scalable Algorithms for Molecular Dynamics Simulations on Commodity Clusters. *Proceedings of the ACM/IEEE Conference on Supercomputing (SC06)* **2006**, Tampa, Florida November 11-17.

